# CONSTITUTIVE EQUATIONS AND PROCESSING MAP FOR HOT DEFORMATION OF A Ti-6Al-4V ALLOY PREPARED WITH SPARK-PLASMA SINTERING

## KONSTITUTIVNE ENAČBE IN NAČRTOVANJE PROCESA VROČE DEFORMACIJE Ti-6Al-4V ZLITINE, IZDELANE S POSTOPKOM ISKRILNO-PLAZEMSKEGA SINTRANJA

**Yaojin Wu[1], Haijun Liu[2], Jian Xu[2], Zhimin Zhang[2], Yong Xue[2]\***

[1]School of Mechanical and Electrical Engineering, North University of China, No. 3 Xueyuan Rd., Taiyuan 030051, China
[2]School of Material Science and Engineering, North University of China, No. 3 Xueyuan Rd., Taiyuan 030051, China

High-temperature flow behaviors of a spark-plasma-sintered Ti-6Al-4V alloy was studied at a temperature range of 850–1050 °C and a strain rate of 0.001–5 s$^{-1}$ on a Gleeble-1500D simulator. The true stress-strain curve of the alloy deformed at the total strain of about 70 % was studied. The results show that the flow stress increased as the deformation temperature decreased and the strain rate increased. Based on an Arrhenius-type equation, a constitutive equation was established. In the constitutive equation, the strain has a significant influence on the material parameters, and the relationships between the material parameters and strain are incorporated with a fine polynomial fitting. So, the flow stress is regarded as the function of the deformation parameters such as strain, strain rate and deformation temperature. The average activation energy for the hot deformation of the spark-plasma-sintered Ti-6Al-4V alloy was 425.581 kJ/mol. Meanwhile, hot-processing maps were established based on dynamic material modeling to obtain the regular pattern of the influence of the processing parameters on deformation. The results show that the effects of deformation temperature, strain rate and strain on the peak-dissipation efficiency factor and the instability range are extremely significant. With an increase in the strain, the peak-dissipation efficiency factor increases and the flow-instability range gradually decreases. The optimum deformation temperature and strain rate for hot working of the spark-plasma-sintered Ti-6Al-4V alloy are 950–1000 °C and 1–5 s$^{-1}$, respectively.
Keywords: Ti-6Al-4V alloy, hot compression, constitutive model, processing map

Avtorji prispevka so študirali visoko temperaturno plastično tečenje iskrilno-plazemsko sintrane Ti-6Al-4V zlitine v temperaturnem območju med 850 °C in 1050 °C in pri hitrostih deformacije med 0,001 s$^{-1}$ in 5 s$^{-1}$ na simulatorju Gleeble-1500D. Študirali so dobljene krivulje *prava napetost-prava deformacija* za izbrano zlitino pri celokupni deformaciji do ca. 70 %. Rezultati analiz so pokazali, da napetost tečenja raste s padajočo temperaturo deformacije in naraščajočo hitrostjo deformacije. Potrdili so, da konstiutivna enačba procesa poteka v skladu z Arrheniusovim tipom enačbe. V njej ima deformacija pomemben vpliv na materialne parametre. V enačbo med materialnimi parametri in deformacijo so vključili povezavo, ki so jo dobili s finim polinomskim fitanjem oz. prilagajanjem podatkov. Tako je napetost tečenja odvisna od deformacijskih parametrov, kot so: deformacija, hitrost in temperatura deformacije. Ugotovili do, da je povprečna aktivacijska energija za vročo deformacijo iskrilno-plazemsko sintrane Ti-6Al-4V zlitine enaka 425,581 kJ/mol. Za načrtovanje in ugotovitev poteka procesa so uporabili dinamično modeliranje materiala z upoštevanjem zakonitih vzorcev, ki vplivajo na procesne parametre deformacije. Rezultati študije so pokazali, da so vplivi temperature in hitrosti deformacije ter same deformacije na vršni faktor disipacijske učinkovitosti in območje nestabilnosti ekstremno pomembni. S povečevanjem deformacije se postopno povečuje vršni faktor disipacijske učinkovitosti in zmanjšuje območje nestabilnosti plastičnega tečenja. Ugotovili so, da se optimalni deformacijski parameter za temperaturo in hitrost deformacije za vročo plastično deformacijo iskrilno-plazemsko sintrane Ti-6Al-4V zlitine nahaja med 950 °C in 1000 °C ter med 1 s$^{-1}$ in 5 s$^{-1}$.
Ključne besede: Ti-6Al-4V zlitina, vroče zgoščevanje pod tlakom, konstitutivni model, načrtovanje in potek procesa

## 1 INTRODUCTION

The two-phase($\alpha$+$\beta$) titanium alloy, especially the Ti-6Al-4V alloy, is famous for its favorable comprehensive properties such as high strength and stiffness, low density, good corrosion resistance, reasonable ductility and high-temperature properties.[1] Due to its excellent performance, the Ti-6Al-4V alloy is applied in the aerospace industry to manufacture aero-engines and turbine blades. The development of modern science and technology has higher requirements for material pro-

cessing and performance, involving integral forming, rapid prototyping and high-strength forming. However, the traditional casting and forging techniques used for integral forming usually generate a series of issues relating to the bulk microstructure, shrinkage-cavity defects and composition segregation, resulting in a low ductility and poor in-use stability of the final component. Although the mechanical properties of titanium-alloy forgings are better than those of castings, the forging technology is more about forming simple structures. It also wastes more materials, which leads to higher costs.[2,3]

In order to overcome these problems, the powder-metallurgy technology, which has several advantages

*Corresponding author's e-mail:
YongXue395@163.com (Yong Xue)

such as remarkable energy saving, material saving, excellent performance, high-product precision and good stability is introduced. In addition, some materials and complex parts, which cannot be prepared with the traditional casting method and mechanical processing method can also be manufactured with the powder-metallurgy technology.[4,5] C. Liang et al.[6] used hydrogenation/dehydrogenation powder sintering combined with the forging method to prepare a Ti-6Al-4V alloy with a lamellar structure and close to 100 % density. After the forging, the tensile strength of the Ti-6Al-4V alloy can reach 1350 MPa, the yield strength is 1200 MPa, the elongation reaches 10 % and the size of internal particles is less than 3 μm. Compared with cold-pressing sintering, hot pressing and hot isostatic pressing, spark-plasma sintering (SPS) is a new powder-metallurgy sintering technology, whose characteristics include a fast heating rate, short sintering time, controllable structure and uniform density. SPS can effectively suppress the growth of sintered grains and obtain uniform blocks with a fine microstructure, and it also provides sufficient energy and time for the grain growth and phase transformation which can control the evolution of the microstructure to achieve a higher performance.

However, as the alloys produced with SPS are not fully dense, a study was carried out suggesting that the sintering density can be controlled by controlling the deformation parameters.[7] But there are few reports about the deformation behavior of a Ti-6Al-4V alloy SPSed at a high temperature, and the relevant forging-process design also lacks the corresponding theoretical basis. Therefore, it is particularly important to research the effect of deformation parameters for the SPSed Ti-6Al-4V alloy in order to obtain better properties during a forging process. Hot deformation of titanium alloys is accompanied by complex physical processes such as work hardening, dynamic recovery, rheological softening and dynamic recrystallization, which have important impacts on the microstructure and properties of materials. So, it is important to study the thermal-deformation mechanism of the SPSed Ti-6Al-4V alloy to find the optimum processing parameters and clearly understand the flow behavior at elevated temperatures.[8]

The constitutive equation was developed as an input to the finite-element code to simulate the evolution of the microstructure during a thermal-deformation process.[9] Therefore, the accuracy of the constitutive equation determines the accuracy of the simulation. Usually, the constitutive relation is a function of thermal-deformation parameters such as deformation temperature, strain rate and true strain.[10] M. Wang et al.[11] studied the hot-deformation behavior of a powdered isostatically pressed Ti-6Al-4V alloy and constructed the constitutive equations of two-phase and single-phase regions. Based on a dynamic-material model (DMM), a hot-processing map combined with a power-dissipation map and

instability map is derived. The instability map is mainly used to select suitable processing parameters (deformation temperature and strain rate) and the power-dissipation map indicates the stability of material deformation. So, the hot-processing map can clarify the deformation mechanism of the material at different temperatures and strain rates, and can also provide a theoretical basis for the thermal processing.[12,13] Moreover, the safe deformation domain of a perfect thermal-processing performance and high power-dissipation factor can be obtained with the hot-processing map. Although a lot of work was carried out to analyze the hot-flow mechanism of a titanium alloy, combined with a hot-processing map, the thermal deformation of a SPSed Ti-6Al-4V alloy is rare.

In this work, Ti-6Al-4V alloy powder was near-net formed due to spark-plasma sintering (SPS) and a hot-compression test was carried out. Then, the characteristics of the true stress-strain curve and the effects of hot-deformation parameters on the microstructure were analyzed. Based on the hot-deformation behavior of the SPSed Ti-6Al-4V alloy, the suitable constitutive equation and hot-processing map were established for this alloy. The study provides a reasonable parameter basis for a finite-element numerical simulation and forging modification of a Ti-6Al-4V alloy complex-component powder-body multi-directional load forming, which provides practical information for future applications.

## 2 METHODS AND EXPERIMENTAL PART

The hot-compression material used in this experiment was a spark-plasma-sintered Ti-6Al-4V alloy and its chemical composition is shown in **Table 1**. Experimental samples were obtained with spark-plasma sintering at a temperature of 900 °C and a pressure of 30 MPa applied for 5 minutes and then air-cooled to room temperature. Their dimensions were $\phi 30 \times 18$ mm. The microstructure of the alloy is shown in **Figure 1**. Hot-compression samples were cut from it, having dimension of $\phi 8 \times 12$ mm and hot compression was carried out on a Gleeble-1500 thermo-simulation machine in a deformation-temperature and strain-rate range of 850–1050 °C and 0.001–5 s⁻¹, respectively. All hot-compression specimens were deformed to the maximum deformation of about 70 %. Then, all the samples were immediately quenched in cold water to obtain deformation microstructures and the microstructure of the hot-compression samples was observed using optical microscopy. The etching solution included 1 vol.% HF + 3vol.% $HNO_3$+ 7vol.% $C_2H_6O$.

**Table 1:** Chemical composition of TC4 titanium alloy (mass fractions, %)

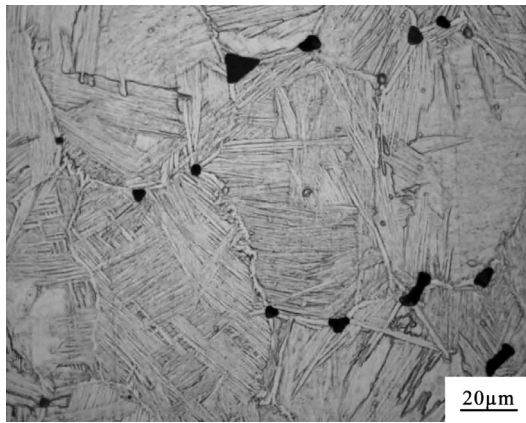| C | H | O | N | Fe | Al | V | Ti |
|---|---|---|---|----|----|----|----|
| 0.005 | 0.02 | 0.44 | 0.021 | 0.04 | 6.06 | 4.02 | Bal. |

**Figure 1:** Microstructure of SPSed TC4 titanium alloy before hot-compression deformation

### 2.1. Flow-stress behavior during hot deformation

**Figure 2** shows the true stress-strain curves of the spark-plasma-sintered Ti-6Al-4V alloy at different deformation temperatures of (850, 950 and 1050) °C in the strain-rate range of 0.001–5 s⁻¹. As shown by the figure, with an increase in the deformation temperature and a decrease in the strain rate, the flow stress decreases significantly, indicating that the flow stress is affected by the deformation temperature and strain rate. Another similar phenomenon is also observed in **Figure 2**: due to the advantages of work hardening, the flow-stress value suddenly increases to its peak during the initial stage of the deformation process, which is mainly due to an increase in dislocations. As the strain increases further, the flow-stress value becomes steady after having reached the peak value, which is due to the balance between work hardening and softening caused by dynamic recovery and recrystallization.[14]

It can be seen that as the deformation temperature decreases, the strain rate increases and the slope of the flow curve increases, which indicates that the work-hardening effect is remarkable at a high strain rate and low temperature, and the softening effect is dominant at a high temperature and low strain rate. Higher temperatures and lower strain rates provide a longer time for

energy accumulation and a higher mobility at the boundaries causing the nucleation and growth of dynamically recrystallized grains and dislocation annihilation, thereby reducing the level of the flow stress.[15]

### 2.2 Establishment of the constitutive equation

Based on the characteristics of the flow curves, it is found that the flow stress of the SPSed Ti-6Al-4V alloy during the hot-compression process is associated with the deformation parameters of strain rate and temperature. Then, the effects of deformation parameters on the deformation behavior of metals can be expressed with an Arrhenius-type equation.[16] In accordance with different stress values, the relationships of the temperature, strain rate and stress can be expressed with the following three equations:

$$\dot{\varepsilon} = A_1 \sigma^{n_1} \exp\left(-\frac{Q}{RT}\right) \quad \alpha\sigma < 0.8 \tag{1}$$

$$\dot{\varepsilon} = A_2 \exp(\beta\sigma) \exp\left(-\frac{Q}{RT}\right) \quad \alpha\sigma > 1.2 \tag{2}$$

$$\dot{\varepsilon} = A[\sinh(\alpha\sigma)]^n \exp\left(-\frac{Q}{RT}\right) \quad \text{for all } \alpha\sigma \tag{3}$$

Here, $\dot{\varepsilon}$, $Q$, $\sigma$, $T$ and $R$ are the strain rate (s⁻¹), activation energy (KJ/mol), stress value (MPa), absolute temperature (K) and universal gas constant (8.3145 J mol⁻¹K⁻¹), respectively. A, $A_1$, $A_2$, $n_1$, $\beta$, $n$ and $\alpha$ are the material constants; $\alpha = \beta/n_1$. Taking natural logarithms on both sides of Equations (1) and (2), the derived formulas are as follows:

$$\ln\dot{\varepsilon} = \ln A_1 + n_1 \ln\sigma - \frac{Q}{RT} \tag{4}$$

$$\ln\dot{\varepsilon} = \ln A_2 + \beta\sigma - \frac{Q}{RT} \tag{5}$$

**Figure 3** shows the relationship between $\ln\sigma - \ln\dot{\varepsilon}$ and $\sigma - \ln\dot{\varepsilon}$ at a true strain of 0.1. Then, material constants $\beta$ and $n_1$ can be calculated from the slopes of the liner fitting of the $\ln\sigma - \ln\dot{\varepsilon}$ plot and $\sigma - \ln\dot{\varepsilon}$ plot where $n_1$ and $\beta$ represent the average values of the slope coefficients, respectively. The values of $n_1$ and $\beta$ are
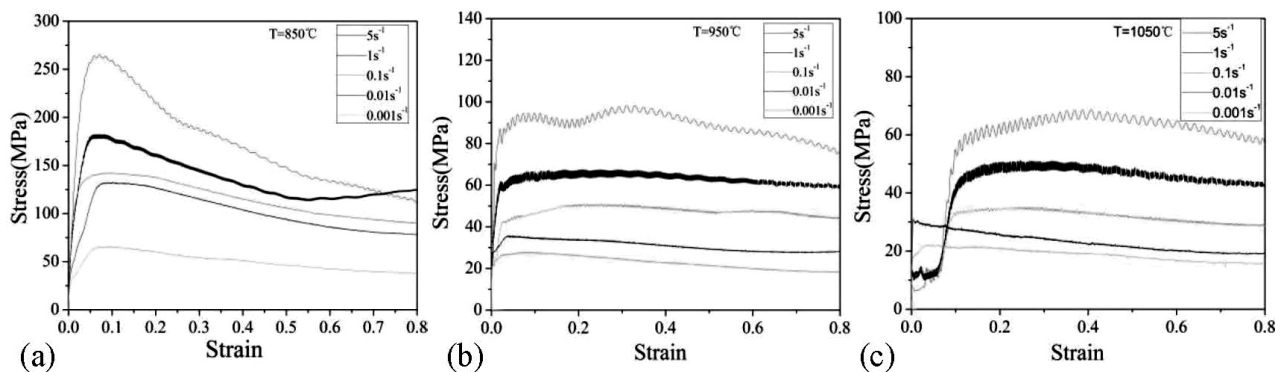


**Figure 2:** True stress-strain curves of SPSed TC4 titanium alloy obtained at: a) 850 °C, b) 950 °C and c) 1050 °C and various strain rates
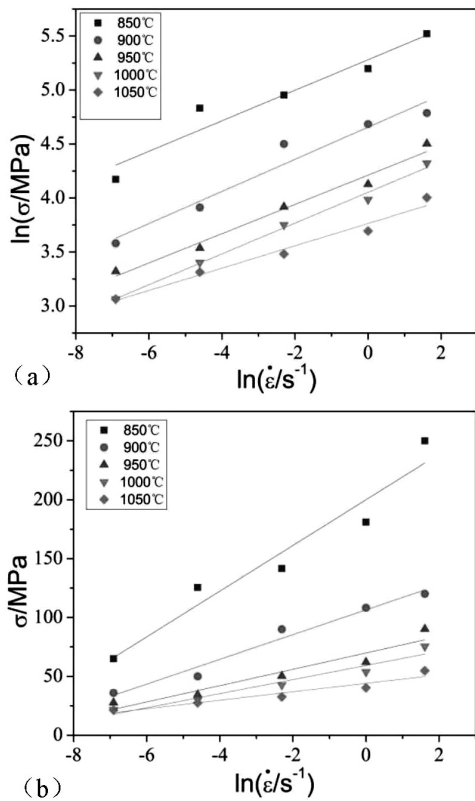
(a)



(b)

**Figure 3:** Relationship between strain rates and deformation temperatures at a strain of 0.1: a) $\ln \sigma_{0.1} - \ln \dot{\varepsilon}$, b) $\sigma_{0.1} - \ln \dot{\varepsilon}$
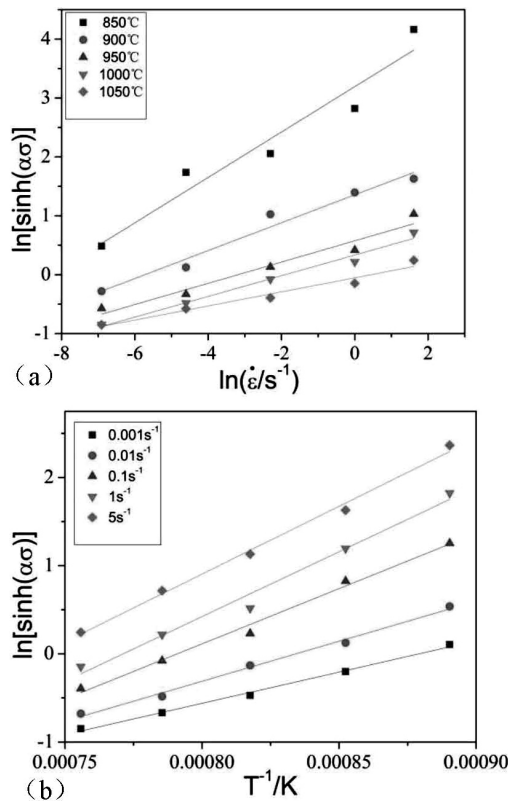


(a)



(b)

**Figure 4:** Relationship between ln sinh ($\alpha\sigma$) – ln $\dot{\varepsilon}$ and ln sinh ($\alpha\sigma$) – $1/T$ of SPSed TC4 titanium alloy at different strain rates: a) ln sinh ($\alpha\sigma$) – ln $\dot{\varepsilon}$, b) ln sinh ($\alpha\sigma$) – $1/T$

deduced to be 7.5701 and 0.1470, based on the best fitting lines from the plots. So, the value of $\alpha$ can be gained in accordance with $\alpha = \beta/n_1 \approx 0.0194$ MPa$^{-1}$. Taking the logarithm of the two sides of Equation (3), the formula is as follows:

$$\ln \dot{\varepsilon} = \ln A - \frac{Q}{RT} + n \ln[\sinh(\alpha\sigma)] \qquad (6)$$

One of the significant deformation parameters, which indicate plastic deformability, is the activation energy ($Q$) that can be obtained from Equation (6):

$$Q = R \left\{ \frac{\partial \ln \dot{\varepsilon}}{\partial \ln[\sinh(\alpha\sigma)]} \right\}_T \left\{ \frac{\partial \ln[\sinh(\alpha\sigma)]}{\partial(1/T)} \right\}_{\dot{\varepsilon}} \qquad (7)$$

**Figure 4** shows the relationship between $\ln[\sinh(\alpha\sigma)]$ and $\ln \dot{\varepsilon}$ at different temperatures as well as $\ln[\sinh(\alpha\sigma)]$ and $1/T$ at different strain rates. So, the average activation energy ($Q$) of the SPSed Ti-6Al-4V alloy, which can be calculated from Equation (7), is 486.889 kJ/mol.

Based on the Zener-Holloman parameter (Z)[17], Equation (3) can be accurately revised as follows:

$$Z = \dot{\varepsilon} \exp\left(\frac{Q}{RT}\right) = A[\sinh(\alpha\sigma)]^n \qquad (8)$$

$$\sigma = \frac{1}{\alpha} \ln \left\{ \left(\frac{Z}{A}\right)^{\frac{1}{n}} + \left[ \left(\frac{Z}{A}\right)^{\frac{2}{n}} + 1 \right]^{\frac{1}{2}} \right\} \qquad (9)$$

Taking the logarithm of the two sides of Equation (8), the formula is as follows:

$$\ln Z = \ln A + n \ln[\sinh(\alpha\sigma)] \qquad (10)$$

The relationship between $\ln Z$ and $\ln[\sinh(\alpha\sigma)]$ is illustrated in **Figure 5**. For evaluating the $n$ value and $\ln A$, index coefficient n is 4.579; the intercept of the fitted curve in **Figure 5** is $\ln A = 44.186$ where $A$ is $1.54848 \times 10^{19}$ s$^{-1}$. Based on the above calculations, the constitutive equations for the flow stress of the Ti-6Al-4V
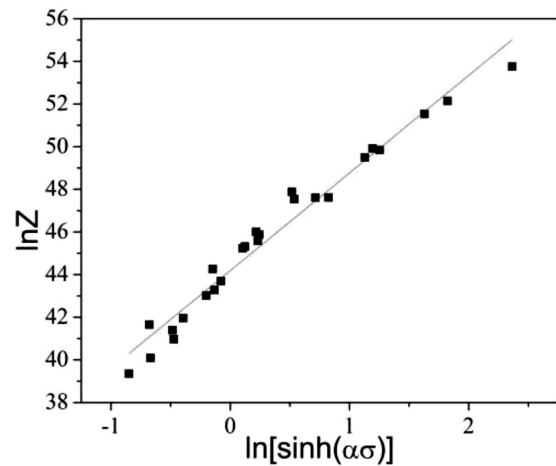


**Figure 5:** Relationship between $\ln Z$ and $\ln[\sinh(\alpha\sigma)]$

alloy with respect to the $T$ function under the true strain of 0.1 can be written as:

$$\dot{\varepsilon}\exp\left(\frac{486889}{RT}\right)=1.54848\times10^{19}\left[\sinh(0.0194\sigma)\right]^{4.579} \quad (11)$$

$$\sigma_{0.1} = \frac{1}{0.0194}\ln\left\{\left(\frac{Z}{1.54\times10^{19}}\right)^{\frac{1}{4.579}}+\left[\left(\frac{Z}{1.54\times10^{19}}\right)^{\frac{2}{4.579}}+1\right]^{\frac{1}{2}}\right\} \quad (12)$$

However, due to the lack of the strain term, Equation (10) does not express the effect of the strain on the flow stress during the thermal-compression process. As can be seen from **Figure 2**, the strain has a significant effect on the flow stress throughout the entire strain interval. Therefore, strain compensation should be considered to derive accurate constitutive equations for predicting the flow behavior. It is important that the constitutive model describes the relationships between the strain rate, temperature and strain. So, the material constants (n, $\alpha$, $Q$ and $A$) at different strains were calculated in accordance with the above methods, and the relationships between the material constants and strain were plotted as shown in **Figure 6**. According to the analysis results, the average deformation activation energy $Q$ of the Ti-6Al-4V alloy is 425.581 kJ/mol at deformation temperatures of 850–1050 °C and strain rates of 0.001–5 s⁻¹.

According to the fitting effect, the result shows that the 5th order of the polynomial was found to represent a good fitting effect between the strain and material constants (*n*, $\alpha$, ln *A*, and *Q*) of the SPSed Ti-6Al-4V alloy as shown in **Figure 6**. So, the Arrhhenius constitutive equation considering the strain can be obtained by substituting material constants nε, αε, Qε and Aε into Equation (3):

$$\dot{\varepsilon}=A\left[\sinh(\alpha_{\varepsilon}\sigma)\right]^{n_{\varepsilon}}\exp\left(-\frac{Q_{\varepsilon}}{RT}\right) \quad (13)$$

where $n_{\varepsilon}$, $\alpha_{\varepsilon}$, $Q_{\varepsilon}$ and $A\varepsilon$ are the material constants of the SPSed TC4 titanium alloy considering the effect of the strain on the flow stress during hot compression.

$n_{\varepsilon} = -389.80\ \varepsilon^5 + 841.24\ \varepsilon^4 + 701.54\ \varepsilon^3 + 282.46\ \varepsilon^2 -$
$- 53.95\ \varepsilon + 7.77$

$\alpha_{\varepsilon} = 0.596\varepsilon^5 - 1.10\ \varepsilon^4 + 0.723\ \varepsilon^3 - 0.182\ \varepsilon^2 +$
$+ 0.012\ \varepsilon + 0.019$

$Q_{\varepsilon} = 24738.672\ \varepsilon^5 - 54473.993\ \varepsilon^4 + 46394.913\ \varepsilon^3 -$
$- 18274.916\ \varepsilon^2 + 2892.433\ \varepsilon + 339.624$

$\ln A_{\varepsilon} = 386.445\ \varepsilon^5 - 1511.471\ \varepsilon^4 + 1932.447\ \varepsilon^3 -$
$- 992.053\ \varepsilon^2 + 174.468\ \varepsilon + 34.912$

### 2.3 Processing map

On the basis of the dynamic material model (DMM) theory, the processing map built by N. Nayan et al.[18] have been widely used as an important tool to analyze the hot-deformation behavior and optimize the hot-working processes. First, the processing map can combine the continuous plastic flow with the microstructure evolution and, secondly, it can be used to describe the dynamic response area during hot deformation. So, the thermal-processing map of SPSed Ti-6Al-4V alloys can be constructed based on a dynamic material model (DMM).[19] The total power dissipation P dissipated by a workpiece during plastic deformation is made up of two complementary parts, *G* and *J*. The *G* dissipation content
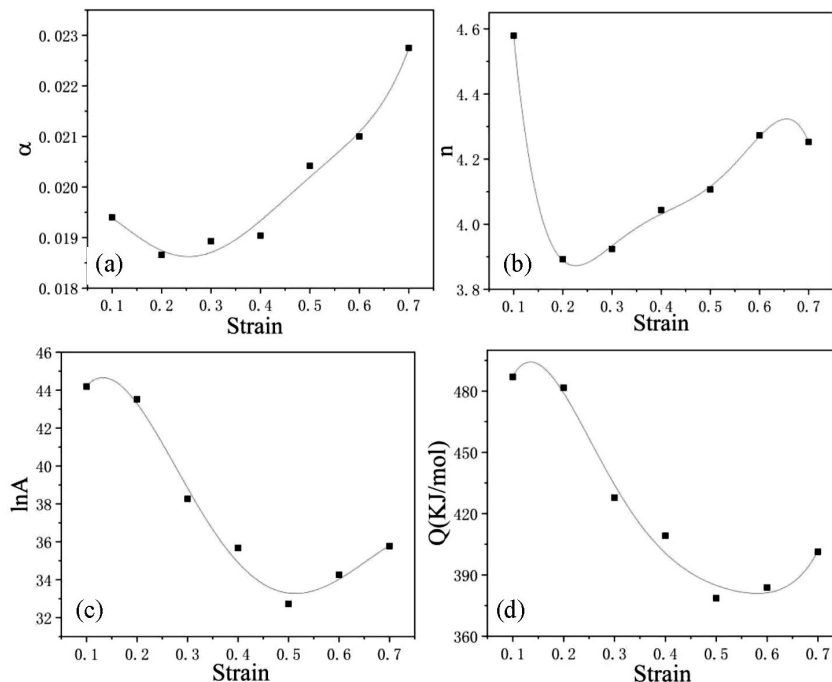


**Figure 6:** Variations in constitutive parameters as a function of strain: a) $\alpha$, b) *n*, c) ln *A*, d) *Q*

dissipated by the plastic deformation of a material and the $J$ co-content represent the dissipation of the microstructure evolution. During hot deformation, the total power dissipation $P$ can be expressed as[20]:

$$P = \sigma \cdot \varepsilon = G + J = \int_0^{\dot{\varepsilon}} \sigma \mathrm{d}\dot{\varepsilon} + \int_0^{\sigma} \dot{\varepsilon} \mathrm{d}\sigma \qquad (14)$$

The strain-rate sensitivity index m and the distribution relationship between $G$ and $J$ are as follows:

$$m = \frac{\partial J}{\partial G} = \frac{\dot{\varepsilon}}{\sigma} \frac{\partial \sigma}{\partial \dot{\varepsilon}} = \frac{\partial \ln \sigma}{\partial \ln \dot{\varepsilon}} \qquad (15)$$

The $J$ co-content can be expressed as $J = (m/m+1)\sigma\dot{\varepsilon}$ through integrating. In an ideal linear-dissipation process, the strain-rate sensitivity index m and the $J$ co-content can be expressed with $m = 1$ and $J = J_{max} = \sigma\dot{\varepsilon}/2$. Therefore, the material power-dissipation efficiency $\eta$ can be expressed as:

$$\eta = \frac{J}{J_{max}} = \frac{2m}{m+1} \qquad (16)$$

where the material power-dissipation efficiency $\eta$ describes different microstructure evolutions of a material under different deformation temperatures and strain rates, such as dynamic recrystallization, dynamic recovery, superplasticity etc. The $\eta$ varies with the strain rate and temperature, providing for power-dissipation maps for different regions, which are directly related to specific microstructures. The material-deformation process, dynamic recrystallization, dynamic recovery and superplasticity are favorable types of material deformation, but the formations of defects such as voids and cracks are harmful deformation mechanisms that must be avoided during the processing. In order to optimize the processability of a material and control the microstructure during the processing, it is important to maintain suitable parameters. Therefore, the temperature and strain rate corresponding to the energy-dissipation peaks in different regions are optimized processing parameters.

In the dynamic material model, the principle of processing instability is established on the basis of the principle of the maximum entropy-generation rate. According to the maximum principle of irreversible thermodynamics, the principle of processing instability can be obtained as[21]:

$$\xi(\dot{\varepsilon}) = \frac{\partial \ln(m/(m+1))}{\partial \ln \dot{\varepsilon}} + m < 0 \qquad (17)$$

The $\xi$ is the instability parameter, which is a function of the deformation temperature and strain rate. The flow-instability map can be obtained from the variation in the deformation temperature and strain rate. After that, the processing map can be obtained by combing the power-dissipation map and instability map. According to the processing maps, the favorable microstructure and properties are obtained by optimizing the process at a strain rate of 0.001–5s$^{-1}$ and deformation temperature of 850–1050°C. Thus, the processing map reflects the influence of the hot-processing parameters on the dissipation-efficiency factor and the instability state, also helping us to avoid the instability region and select the optimal hot-processing parameters.[22] Therefore, the hot-processing maps used for obtaining the optimized hot-processing parameters are of vital importance.

For the titanium alloy subjected to DRX during the hot-deformation process, the flow stress increased to its maximum value, then decreased and finally attained a steady state, which was also verified in **Figure 2**. Therefore, in the present research, the processing maps for the SPSed Ti-6Al-4V alloy at strains of 0.3, 0.5 and 0.7 were investigated, and they showed a steady-state flow.

**Figure 7** shows the processing maps of the SPSed Ti-6Al-4V alloy at the strains of 0.3, 0.5 and 0.7. It can be seen from **Figure 7** that the influence of the strain on the peak-dissipation efficiency factor $\eta$ and the instability regions is extremely significant, and the peak-dissipation efficiency factor $\eta$ and the instability regions show regular changes. As the strain increases, an instability region begins to expand toward the region of high temperature and low strain rate, and it gradually changes from one instability region to three instability regions, while the peak-dissipation efficiency factor $\eta$ remains at the high-temperature and high-strain-rate region.
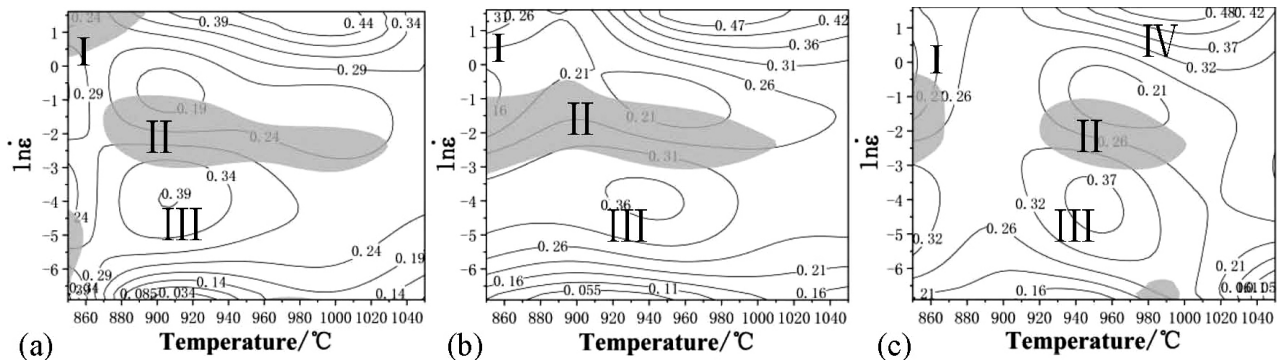


**Figure 7:** Processing maps at different strains: a) $\varepsilon = 0.3$, b) $\varepsilon = 0.5$, c) $\varepsilon = 0.7$
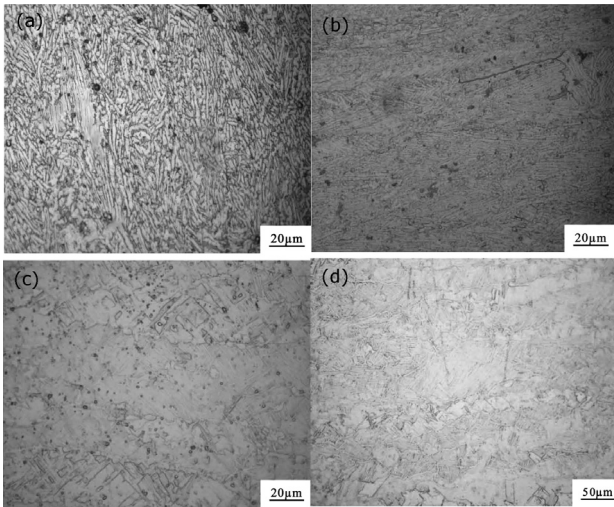
**Figure 8:** Microstructures of SPSed TC4 titanium alloy at different temperatures and strains: a) 850 °C, 1 s$^{-1}$, b) 900 °C, 0.1 s$^{-1}$, c) 950 °C, 0.01 s$^{-1}$, d) 950 °C, 1 s$^{-1}$

At the dominant strain of 0.3, it is evident that the instability is very easy to occur at high strain rates and low temperatures due to the local temperature increase of the material, which results in an adiabatic shear band and stress concentration, and makes most of the energy transform into heat energy. At this time, the power-dissipation efficiency $\eta$ is low and the hot-working performance of the material decreases sharply. Thus, this region should be avoided when the processing parameters are formulated. It is also seen from **Figure 7** that the instability is likely to occur at a high strain rate, like in Domain II, due to the hot energy converted from a large amount of plastic work and the stress concentration caused by an interface slip, not released in time, resulting in instability such as a local flow or cracking.[20]

According to the instability region and peak-dissipation efficiency factor $\eta$, the processing map with the strain of 0.7 can be divided into four parts. Deformation conditions corresponding to Domains I and II include the deformation temperature of 850–900 °C and strain rate of 0.1–5 s$^{-1}$, and the deformation temperature of 900–1000 °C and strain rate of 0.05–0.1 s$^{-1}$, respectively. The two parts are located in the flow-instability region of hot compression and the peak-dissipation efficiency factors are 0.26 and 0.32, respectively; however, it cannot be used as the optimal thermal-deformation region of the SPSed Ti-6Al-4V alloy. **Figures 8a** and **8b** show the microstructures at the deformation temperature of 850 °C and strain rate of 1 s$^{-1}$, and the deformation temperature of 900 °C and the strain rate of 0.1s$^{-1}$, respectively. It can be seen from **Figures 8a** and **8b** that the microstructures deformed under these conditions have an adiabatic shear band and a microcrack, indicating a flow-instability phenomenon.

Domain III is formed at the deformation temperature of 900–960 °C and strain rate of 0.001–0.05 s$^{-1}$ and the dissipation efficiency factor $\eta$ ranges from 0.16 to 0.37

where 0.37 is the peak-dissipation efficiency factor at the strain of 0.7. From **Figure 8c**, it can be seen that new grains were formed and dynamic recrystallization obviously took place after the deformation. In addition, fibrous elongated grains appear in the figure and their number is higher than that of the recrystallized grains. This indicates that the dynamic recovery and dynamic recrystallization of the SPSed Ti-6Al-4V alloy occur under these conditions, and that dynamic recrystallization dominates the deformation process. Dynamic recrystallization and dynamic recovery are favorable hot-working deformation mechanisms, which can improve the hot workability of the alloy. However, it can be seen from **Figure 8c** that the size of dynamically recrystallized grains produced under these conditions is extremely uneven, which is disadvantageous to the mechanical properties of the metal due to the coarse grains. Therefore, hot processing is not the best choice in this area.

Domain IV is formed at the deformation temperature of 900–1000 °C and the strain rate of 0.5–5 s$^{-1}$ and the dissipation efficiency factor $\eta$ ranges from 0.21 to 0.48. **Figure 8d** shows the microstructure of the SPSed Ti-6Al-4V alloy formed at the deformation temperature of 950 °C and strain rate of 1 s$^{-1}$. It can be seen from **Figure 8d** that the microstructure of the alloy, after the deformation, revealed widmanstatten colonies, and the refined colonies are observed at the strain rate of 1 s$^{-1}$. This indicates that the $\beta$ phase experienced a dynamic recrystallization. When the strain rate is 1 s$^{-1}$, a lath-like shape and a small amount of globularization are observed on deformed specimens. The refined widmanstatten microstructure not only has good plasticity, impact toughness, fracture toughness and high-cycle-fatigue strength, but also has good heat strength. Compared with a similar equiaxed structure, the refined widmanstatten microstructure exhibits undisputed superiority in terms of heat intensity. It can be seen from the microstructure that the deformation mechanism of the SPSed Ti-6Al-4V alloy under these conditions is a typical dynamic recovery and partial dynamic recrystallization. Based on the microstructural analysis and processing maps, we can conclude that the optimum temperature and strain-rate ranges of the SPSed Ti-6Al-4V alloy for hot working are 950–1000°C and 1–5 s$^{-1}$.

## 3 CONCLUSIONS

In this research, flow curves, a constitutive equation and processing maps were made to characterize the hot-deformation behavior of the SPSed Ti-6Al-4V alloy at different temperatures and strain rates. Based on the constitutive equation and processing map, the following conclusions were obtained:

(1) The strain has a significant influence on the material constant and a mutual relationship is also

incorporated into the constitutive equation with the polynomial fitting of the material constants and strain. So, the constitutive equation for the strain influence on the hot-deformation behavior is established. The constitutive model of the SPSed Ti-6Al-4V alloy is:

$$\dot{\varepsilon} = Z \exp\left(-\frac{Q_\varepsilon}{RT}\right) = A_\varepsilon \left[\sinh(\alpha_\varepsilon \sigma)\right]^{n_\varepsilon} \exp\left(-\frac{Q_\varepsilon}{RT}\right)$$

$$\sigma_\varepsilon = \frac{1}{\alpha_\varepsilon} \ln\left\{ \left(\frac{Z}{A_\varepsilon}\right)^{\frac{1}{n_\varepsilon}} + \left[\left(\frac{Z}{A_\varepsilon}\right)^{\frac{2}{n_\varepsilon}} + 1\right]^{\frac{1}{2}} \right\}$$

$n\varepsilon = -389.80\varepsilon5 + 841.24\varepsilon4 - 701.54\varepsilon3 + 282.46\varepsilon2 - 53.95\varepsilon + 7.77$

$\alpha\varepsilon = 0.596\varepsilon5 - 1.10\varepsilon4 + 0.723\varepsilon3 - 0.182\varepsilon2 + 0.012\varepsilon + 0.019$

$Q\varepsilon = 24738.672\varepsilon5 - 54473.993\varepsilon4 + 46394.913\varepsilon3 - 18274.916\varepsilon2 + 2892.433\varepsilon + 339.624$

$\ln A\varepsilon = 386.445\varepsilon5 - 1511.471\varepsilon4 + 1932.447\varepsilon3 - 992.053\varepsilon2 + 174.468\varepsilon + 34.912$

(2) The effects of the strain on the peak-dissipation efficiency factor and the instability range are extremely significant. With an increase in the strain, the peak-dissipation efficiency factor increases and the flow-instability range gradually decreases. The processing-map analysis shows that the optimum temperature and strain rate for hot working of the SPSed Ti-6Al-4V alloy are 950–1000 °C and 1–5s$^{-1}$.

## Acknowledgments

## 5 REFERENCES

[1] B. G. Yuan, Y. J. Wang, Y. B. Zheng, L. Q. Gong, Hydrogenation Behavior of Ti6Al4V Alloy, Rare Metal Materials and Engineering, 46 (**2017**) 6, 1486–1490, doi:10.1016/S1875- 5372(17)30151-0

[2] I. Sen, S. Tamirisakandala, D. B. Miracle, U. Ramamurty, Microstructural effects on the mechanical behavior of B-modified Tie6Ale4V alloys, Acta Materialia, 55 (**2007**) 15, 4983–4993, doi:10.1016/j.actamat.2007.05.009

[3] R. M. German, Progress in titanium metal powder injection molding, Materials, 6 (**2013**) 8, 3641–3662, doi:10.3390/ma6083641

[4] Z. Trzaska, G. Bonnefont, G. Fantozzi, J. P. Monchoux, Comparison of densification kinetics of a TiAl powder by spark plasma sintering and hot pressing, Acta Materialia, 135 (**2017**), 1–13, doi:10.1016/j.actamat.2017.06.004

[5] P. Novák, H. Moravec, V. Vojtěch, A. Knaislová, A. Školáková, T. F. Kubatík, J. Kopeček, Powder-metallurgy preparation of NiTi shape-memory alloy using mechanical alloying and spark-plasma sintering, Materiali in Tehnologije, 51 (**2017**) 1, 141–144, doi:10.17222/mit.2016.011

[6] C. Liang, M. X. Ma, M. T. Jia, S. Raynova, J. Q.Yan, D. L. Zhang, Microstructures and tensile mechanical properties of Ti-6Al-4V bar/disk fabricated by powder compact extrusion/forging,

[7] Y. Sun, G. Q. Luo, J. Zhang, C. D. Wu, J. Li, Q. Shen, L. M. Zhang, Phase transition, microstructure and mechanical properties of TC4 titanium alloy prepared by plasma activated sintering, Journal of Alloys and Compounds, 741 (**2018**), 918–926, doi:10.1016/j.jallcom. 2018.01.197

Materials Science and Engineering: A, 619 (**2014**), 290–299, doi:10.1016/j.msea.2014. 09.083

[8] Y. Q. Ning, B. C. Xie, H. Q. Liang, H. Li, X. M. Yang, H. Z. Guo, Dynamic softening behavior of TC18 titanium alloy during hot deformation, Materials and Design, 71 (**2015**) 68, doi:10.1016/ j.matdes. 2015.01.009

[9] J. Cai, F. G. Li, T. Y. Liu, B. Chen, M. He, Constitutive equations for elevated temperature flow stress of Ti-6Al-4V alloy considering the effect of strain, Materials and Design, 32 (**2011**) 3, 1144–51, doi:10.1016/j.matdes.2010.11.004

[10] D. Samantaray, S. Mandal, A. K. Bhaduri, S. Venugopal, P. V. Sivaprasad, Analysis and mathematical modelling of elevated temperature flow behaviour of austenitic stainless steels, Materials Science and Engineering: A, 528 (**2011**) 4, 1931–2208, doi:10.1016/ j.msea.2010.11.011

[11] M. Wang, J. X. Zhou, Y. J. Yin, H. Nan, P. J. Xue, Z. X. Tu, Hot deformation behavior of the Ti-6Al-4V alloy prepared by powder hot isostatic pressing, Journal of Alloys and Compounds, 721 (**2017**), 320–332, doi:10.1016/j.jallcom.2017.06.003

[12] A. Mohamadizadeh, A. Zarei-Hanzaki, H. R. Abedi, S. Mehtonen, D. Porter, Hot deformation characterization of duplex low-density steel through 3D processing map development, Materials Characterization, 107 (**2015**), 293–301, doi:10.1016/j.matchar.2015.07.028

[13] Z. Liying, Y. Guanjun, G. Peng, M. Xiaonan, Z. Yongqing, Z. Lian, Processing map of one kind of metastable β titanium alloy, Rare Metal Materials and Engineering, 39 (**2010**) 9, 1505–1508, doi:10.1016/s1875-5372 (10)60119-1

[14] D. Samantaray, S. Mandal, A. K. Bhaduri, Characterization of deformation instability in modified 9Cr-1Mo steel during thermomechanical processing, Materials and Design, 32 (**2011**) 2, 716–22, doi:10.1016/j.matdes.2010.07.038

[15] X. N. Peng, H. Z. Guo, Z. F. Shi, C. Qin, Z. L. Zhao, Constitutive equations for high temperature flow stress of TC4-DT alloy incorporating strain, strain rate and temperature, Materials and Design, 50 (**2013**), 198–206, doi:10.1016/j.matdes. 2013.03.009

[16] J. Jonas, C. M. Sellars, W. J. M. Tegart, Strength and Structure Under Hot-Working Conditions, International Materials Reviews, 14 (**1969**) 1, 1–24, doi:10.1179/mtlr. 1969.14.1.1

[17] C. Zener, J. Hollomom, High speed deformation of metals, Journal of Applied Physics, 15 (**1944**) 22–32

[18] N. Nayan, S. V. S. Narayana Murty, S. Chhangani, A. Prakash, M. J. N. V. Prasad, I. Samajdar, Effect of temperature and strain rate on hot deformation behavior and microstructure of Al-Cu-Li alloy, Journal of Alloy and Compounds, 723 (**2017**), 548–558, doi:10.1016/ j.jallcom.2017.06.16

[19] Y. V. R. K. Prasad, K. P. Rao, Processing maps and rate controlling mechanisms of hot deformation of electrolytic tough pitch copper in the temperature range 300–950 °C, Materials Science and Engineering: A, 391 (**2005**) 1–2, 141–150, doi:10.1016/j.msea.2004. 08.049

[20] Z. W. Shao, X. R. Zhu, R. Wang, J. Wang, Y. D. Xu, B. R. Zhao, G. P. Ling, Hot deformation and processing map of as-homogenized Mg-9Gd-3Y-2Zn-0.5Zr alloy, Materials and Design, 51 (**2013**), 826–832, doi:10.1016/j.matdes. 2013.04.095

[21] Y. V. R. K. Prasad, Processing maps for hot working of titanium alloy, Materials Science and Engineering: A, 243 (**1998**) 1, 82–88, doi:10.1016/S0921- 5093(97)00782-X

[22] H. Y. Sun, J. X. Cao, B. Wang, X. Huang, C. X. Cao, Hot processing map and deformation mechanism of as-cast burn resistant titanium alloy, Rare Metal Materials and Engineering, 42 (**2013**) 12, 2541–2546, doi:10.1016/S1872-5805(13)60093-1